Materials Letters 106 (2013) 405–408

Contents lists available at SciVerse ScienceDirect

Materials Letters

journal homepage: www.elsevier.com/locate/matlet

Dielectric behavior of lead lanthanum zirconate titanate thin films deposited on different electrodes/substrates

Sheng Tong [a,b,c,*], Beihai Ma [b], Manoj Narayanan [b], Shanshan Liu [b], Uthamalingam Balachandran [b], Donglu Shi [a]

[a] College of Engineering and Applied Science, University of Cincinnati, Cincinnati, OH 45221, USA
[b] Energy Systems Division, Argonne National Laboratory, Argonne, IL 60439, USA
[c] Nanoscience and Technology Division, Argonne National Laboratory, Argonne, IL 60439, USA

ARTICLE INFO

Article history:
Received 11 September 2012
Accepted 17 May 2013
Available online 28 May 2013

Keywords:
Thin films
Ferroelectrics
Dielectrics
Deposition
X-ray techniques

ABSTRACT

The dielectric properties of lead lanthanum zirconate titanate (PLZT) thin films are investigated on different combinations of bottom electrode (Pt, $LaNiO_3$) and substrate (Ni, Si). The results indicate strong effects of electrode on the permittivity and dielectric loss of these PLZT thin-films capacitors. The substrate-induced thermal strain has a great impact on the temperature dependence of the dielectric behavior. Based on these findings, dielectric applications using PLZT thin films in a wide range of temperature are possible by selecting appropriate electrodes and substrates.

© 2013 Published by Elsevier B.V.

1. Introduction

There has been extensive research on thin films of ferroelectric materials due to their unique physical and electrical properties for potential applications in ferroelectric memories, tunable microwave devices, and infrared sensors [1–3]. Typically, a ferroelectric thin film is deposited on substrates for physical support. Also widely employed is a metal–ferroelectric–metal (MFM) structure, where a compensating charge is present on each electrode of the polarized ferroelectric layer. Thus, ferroelectric thin films are usually either deposited on a metal substrate (e.g., nickel [4,5], copper [6,7]) or buffered substrates that serve as the bottom electrode (e.g., platinized silicon [3,8]). The dielectric and ferroelectric properties of capacitors, primarily based on ferroelectric compositions, are highly dependent on the bottom electrode and substrate. Due to ferroelastic nature of the thin films [9], substrate-induced strain, mainly thermal strain for polycrystalline films, is critical in determining the dielectric and ferroelectric properties [10]. Moreover, the electrodes play an important role in the electrical behavior of ferroelectric thin-film capacitors [11]. The influence of substrate or bottom electrode on the dielectric properties has been investigated intensively, for example, Refs. [12–17] reported the thermal strain due to substrates on the dielectric properties of $BaTiO_3$, $x Pb(Mg_{1/3}Nb_{2/3})O_3$–$(1-x)PbTiO_3$ (PMN-PT), $Pb(Zr,Ti)O_3$ (PZT), and $(Pb,La)(Zr,Ti)O_3$ (PLZT), and Refs. [18–20] reported the electrode effect on the dielectric properties of $(Pb,La)TiO_3$, PZT, $(Ba,Sr)TiO_3$, PMN, and PLZT. However, the combined-effects of substrate and bottom electrode on the dielectric behavior and phase transition on the ferroelectric thin films have not been reported to our knowledge. In this letter, we report on the effects of the bottom electrode (Pt and $LaNiO_3$) and substrate (Si and Ni) on the dielectric properties of PLZT films. It should be noted that the dielectric properties of ferroelectric thin films is highly dependent on the film thickness at nanoscale, due to increased contribution from "dead layer" effect [21–23]. Therefore, to eliminate such effects, we fabricated constant ~1-μm-thick PLZT films in this work.

2. Material and methods

$Pb_{0.92}La_{0.08}(Zr_{0.52}Ti_{0.48})O_3$ (PLZT) thin films were deposited on substrates of nickel buffered by $LaNiO_3$ (LNO/Ni), silicon buffered by $LaNiO_3$ (LNO/Si), platinized silicon buffered by $LaNiO_3$ (LNO/Pt/Si), and platinized silicon (Pt/Si). Fabrication details on the PLZT and LNO thin films prepared from acetate precursors, including solution preparation, deposition, and heat treatment are reported elsewhere [17,24]. Briefly, a 0.3 M LNO precursor solution was prepared by dissolving an appropriate molar ratio of lanthanum nitrate hexahydrate and nickel acetate tetrahydrate into acetic acid

* Corresponding author at: Nanoscience and Technology Division, Argonne National Laboratory, Argonne, IL 60439, USA. Tel.: +1 630 252 4628; fax: +1 630 252 4646.
E-mail addresses: shengtg@mail.uc.edu (S. Tong), shid@ucmail.uc.edu (D. Shi).

0167-577X/$ - see front matter © 2013 Published by Elsevier B.V.
http://dx.doi.org/10.1016/j.matlet.2013.05.068

and refluxing it at 105 °C for 1.5 h. 0.5 M PLZT solution was prepared by dissolving zirconium n-propoxide, titanium isopropoxide, lead acetate and lanthanum acetate in acetic acid, n-propanol and deionized water (7:7:1 volume ratio) at 105 °C/1 h using inverted mixing order reported by Schwartz [8]. Films were deposited by spinning coating the precursor solutions at 3000 rpm for 30 s, pyrolyzing at 325 °C for 10 min, and crystallizing at 625 °C for 5 min. This process was repeated to achieve films of desired thickness [17,24]. The thickness of the platinum electrode, LNO buffer layer, and PLZT thin films was ~100 nm, ~400 nm, and ~1 µm, respectively. The platinum top electrode (~250-µm diameter) was deposited through a shadow mask by e-beam evaporation. The samples were studied by X-ray diffraction (XRD, Bruker AXS diffractometer) analysis and LCR meter (Agilent E4980A) measurements with a 0.1-V oscillating signal at 10 kHz in conjunction with a Signatone QuieTemp probe station with hot stage (Lucas Signatone Corp., CA).

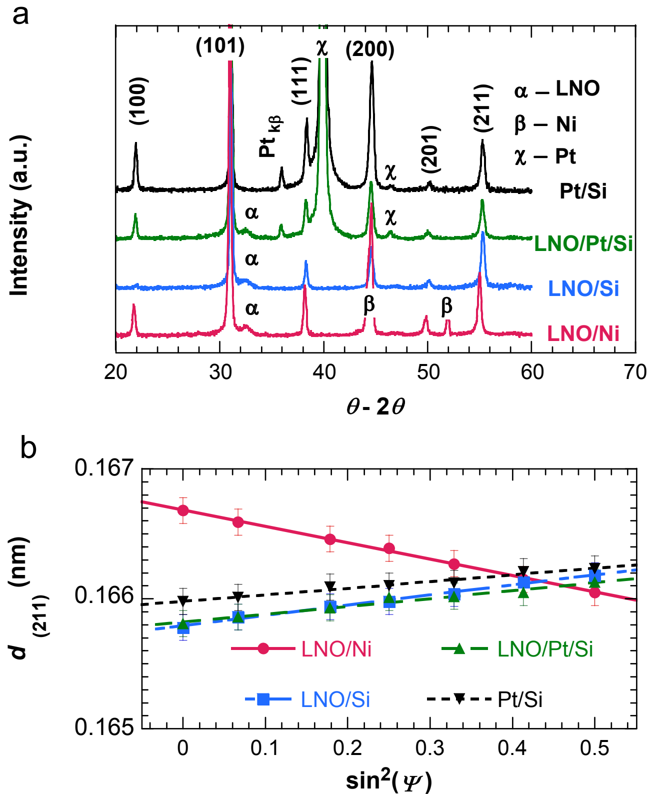

Fig. 1. (a) XRD patterns of the PLZT thin films deposited on various bottom electrodes/substrates. (b) Interplanar spacing $d_{(211)}$ vs. $\sin^2(\Psi)$ of the corresponding PLZT thin films.

3. Results and discussion

The XRD patterns in Fig. 1a indicate the formation of phase-pure perovskite with randomly oriented pseudo-cubic structure in the PLZT thin films deposited on Pt/Si, LNO/Pt/Si, LNO/Si, and LNO/Ni. The ratio of the peak intensities corresponding to the two strongest peaks [(111) and (101)] for the samples was 0.14 ± 0.02 confirming the randomness of the orientation. The strain states of the PLZT thin films are studied by the $\sin^2 \Psi$ method, and the results are shown in Fig. 1b. Lattice spacings (d) are determined from the PLZT (211) reflections with ψ in the range of 0–45°. Small variance ($\pm 0.3\%$) in the d_Ψ vs. $\sin^2 \Psi$ for $\Phi = 0°$, 45°, and 90° (not given in this letter) indicates isotropic and homogeneous in-plane strains of the PLZT thin films, which is common in polycrystalline thin films. The data for d_Ψ vs. $\sin^2 \Psi$ fit to the line shown in Fig. 1b ($R > 0.9848$) and can be mathematically represented as [25]

$$d_\Psi = d_\perp + (d_\angle - d_\perp) \sin^2 \Psi \quad (1)$$

where d_Ψ, $d_\perp$, and $d_\angle$ are the lattice spacing at Ψ, $\Psi = 0$ (out-of-plane), and $\Psi = 90°$ (in-plane), respectively. By applying the strain definition $S = (d - d_0)/d_0$, where d_0 is the strain-free lattice spacing, the relationship between the out-of-plane strain ($S_\perp$) and in-plane strain ($S_\angle$) associated with Poisson's ratio ($\nu = 0.30$ [11]) in Fig. 1b can be expressed as [13]

$$S_\perp = S_\angle \left(-\frac{2\nu}{1-\nu} \right) \quad (2)$$

From Fig. 1b, $d_0(211)$ is calculated to be 0.1662 ± 0.0083 nm (R=0.9995), leading to calculated $S_\angle$ values of $-0.42 \pm 0.02\%$ for LNO/Ni, $0.19 \pm 0.01\%$ for LNO/Si, $0.16 \pm 0.01\%$ for LNO/Pt/Si, and $0.20 \pm 0.01\%$ for Pt/Si. These results suggest that PLZT thin films deposited on nickel substrates are under compressive strain, and those on silicon substrates are under tensile strain, regardless of the buffer layer.

Thermal strain, caused by the thermal expansion coefficient mismatch between the thin film and substrate, is defined as $S_t = \Delta\alpha (T_s - T_0)$, where α is the thermal expansion coefficient, T_s is the sintering temperature, and T_0 is room temperature. Given the parameters [24,26–28] of $\alpha(\text{PLZT}) = 5.4 \times 10^{-6}/°C$, $\alpha(\text{Si}) = 3 \times 10^{-6}/°C$, $\alpha(\text{Ni}) = 13 \times 10^{-6}/°C$, $T_s = 650$ °C, and $T_0 = 25$ °C, S_t is calculated to

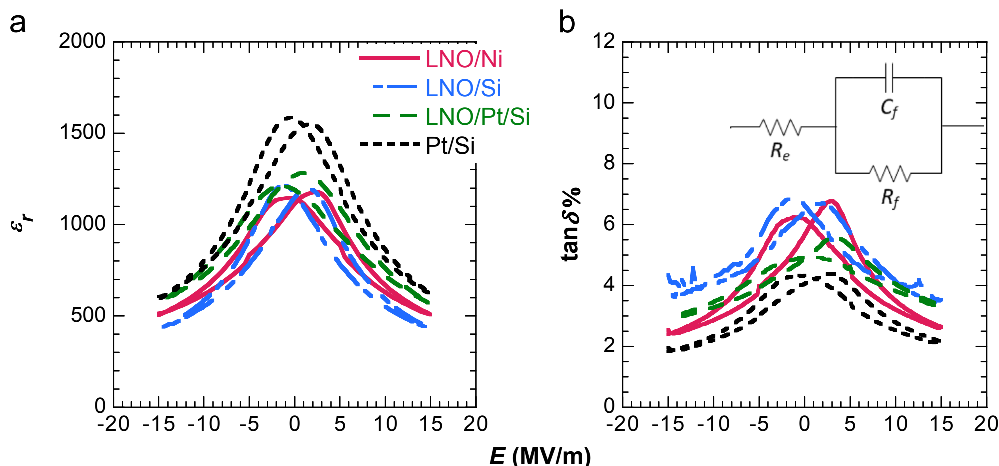

Fig. 2. Room-temperature dielectric responses to DC bias of PLZT thin films deposited on various bottom electrodes/substrates (10 kHz). Inset is the equivalent circuit model of a metal–ferroelectric–metal structure.

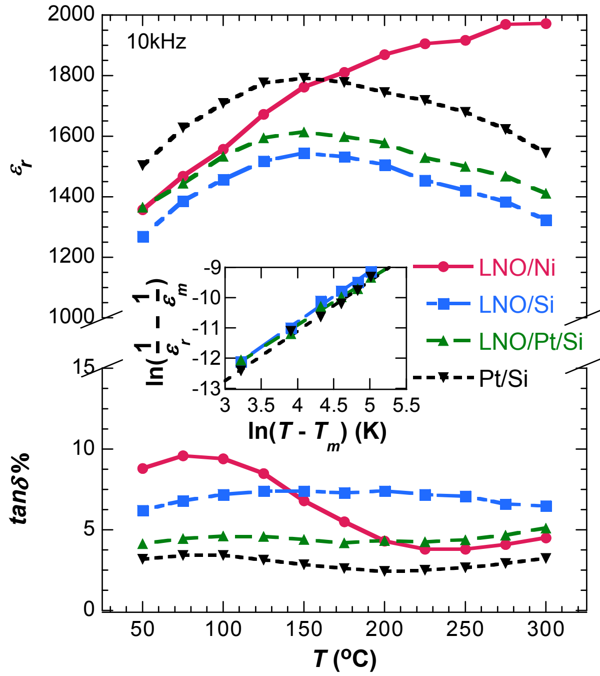

Fig. 3. Temperature-dependent dielectric behavior of PLZT thin films deposited on various substrates. Inset shows the diffuse coefficients fit to data for PLZT thin films deposited on LNO/Si, LNO/Pt/Si, and Pt/Si.

be 0.15% for the Si substrate samples and −0.47% for the Ni substrate samples. On the basis of the measured strains, it is concluded that all the PLZT thin films are mainly under thermal strain. This finding is expected for polycrystalline PLZT thin films, since the ratios of the substrate-to-film thickness (>380) and substrate-to-buffer-layer thickness (>760) are large.

Fig. 2 shows the permittivity (ε_r) and dielectric loss ($\tan\delta$) vs. DC bias at 10 kHz for the PLZT thin-film capacitors. The butterfly-shaped *C–V* curves are typically seen in ferroelectric thin films. The zero-bias permittivity of PLZT thin-film capacitors is high, LNO/Si (1160)≈LNO/Ni (1140) < LNO/Pt/Si (1230) < Pt/Si (1500), and the dielectric loss is low, LNO/Si (6.4%) > LNO/Ni (5.7%) > LNO/Pt/Si (4.9%) > Pt/Si (4.1%). These results indicate that the dielectric properties of the thin-film capacitors are highly dependent on the conductive properties of the bottom electrodes.

The measured permittivity ε_{rm} and dielectric loss $\tan\delta_m$ of an ideal ferroelectric structure are determined from an equivalent circuit (EC) consisting of a capacitor (C_m) and a resistor (R_m) in parallel. The $\varepsilon_{rm}=C_m d/(A\varepsilon_0)$, where d is thickness of the thin film, A the electrode size, and ε_0 the vacuum permittivity, and the $\tan\delta_m=1/(\omega R_m C_m)$, where ω is angular frequency. With this EC, however, the electrode contribution to the permittivity and dielectric loss is not included. To explain the electrode effect on the dielectric properties, a more appropriate EC for MFM structure is shown in the inset of Fig. 2 to determine the true dielectric properties of the PLZT thin films. This EC involves an ideal ferroelectric structure (C_f and R_f in parallel) in series with a resistor (R_e) corresponding to the electrode. Comparing equivalent parallel circuit and model circuit in inset of Fig. 2, the following equations for the thin film with electrode contribution apply [18]:

$$\varepsilon_{rm}=\frac{\varepsilon_{rf}}{(1+r)^2+(r\tan^{-1}\delta_f)^2} \tag{3}$$

$$\tan\delta_m=\tan\delta_f+r(\tan\delta_f+\tan^{-1}\delta_f) \tag{4}$$

where ε_{rf} and $\tan\delta_f$ are true permittivity and dielectric loss of the ferroelectric thin films (electrode resistance independent), $r=R_e/R_f$.

For small electrode thicknesses, the electrode contact resistance cannot be ignored, and would increase r [19]. Therefore, based on Eqs. (3) and (4) when r increases, ε_{rm} decreases while $\tan\delta_m$ increases, compared to ε_{rf} and $\tan\delta_f$, when $r=0$. The bottom electrode resistivity values ρ(Ni)≈6.93 μΩ cm [28], ρ(Pt)≈10.5 μΩ cm [28], and ρ(LNO)≈1720 μΩ cm (tested using four-point probe method). This wide range of resistance is consistent with the measured permittivity and dielectric loss for the PLZT films deposited on LNO/Si, LNO/Ni, LNO/Pt/Si, and Pt/Si.

The dielectric properties of the samples with PLZT thin films are illustrated in Fig. 3 as a function of temperature. The ε_r–T curves for PLZT deposited on the LNO/Ni substrate increase steadily over the temperature range, while those for PLZT deposited on the silicon substrate shows a unique peak (T_m) at ~150 °C. The permittivity peak temperature shift is mainly induced by the thermal strain from the substrates [13,22,29]. $\tan\delta$ of the PLZT thin films does not exhibit drastic variations corresponding to the permittivity peaks, with only minor changes ($<7\%$) in the temperature range. As a relaxor, PLZT undergoes a diffused phase transition around T_m, and permittivity above T_m obeys the Curie–Weiss type law, as follows [1]:

$$\frac{1}{\varepsilon_r}-\frac{1}{\varepsilon_m}=C(T-T_m)^n \tag{5}$$

where ε_m is the peak permittivity, C is a constant, and n is a dispersion factor between 1 and 2. The n value in Eq. 5 for the PLZT thin films on Pt/Si, LNO/Pt/Si, and LNO/Si is determined from the slope of the lines in the inset of Fig. 3, and is found to be 1.62 ± 0.06 ($R=0.996$). Although the permittivity peak values (ε_m) vary according to the bottom electrode used (1540 for LNO/Si, 1610 for LNO/Pt/Si, and 1790 for Pt/Si), the same silicon substrate for these samples yields the same T_m and n values, indicating that these parameters are highly related to thermal strain. Previous studies mainly focused on the magnitude of the permittivity peak shift due to the thermal strain [13,22,29]. In this letter we highlight the combined effects of thermal strain and electrode on the dielectric response and its thermal behavior.

4. Conclusions

We have investigated the strains and dielectric properties of PLZT thin films deposited on different bottom electrodes/substrates. While the conductive properties of the bottom electrodes determine the absolute values of permittivity and dielectric loss of these ferroelectric thin-film capacitors, the substrate-induced thermal strain is essential in modifying the peak and shape of temperature-dependent permittivity curves. Thus, it is possible to tune the dielectric behavior of ferroelectric thin-film capacitors over a wide temperature range by selecting the proper combination of bottom electrode and substrate.

Acknowledgments

This work was supported by the US Department of Energy, Vehicle Technologies Program, under Contract DE-AC02-06CH11357.

References

[1] Cross LE. Relaxor ferroelectrics. In: Heywang Walter, Lubitz Karl, Wersing Wolfram, editors. Piezoelectricity; 2008. p. 131–55.
[2] Scott JF. Science 2007;315:954.
[3] Setter N, Damjanovic D, Eng L, et al. J Appl Phys 2006;100:051606.
[4] Zou Q, Ruda HE, Yacobi BG. Appl Phys Lett 2001;78:1282.
[5] Narayanan M, Ma B, Tong S, et al. Int J Appl Ceram Technol 2011.
[6] Kingon AI, Srinivasan S. Nat Mater 2005;4:233–7.

[7] Narayanan M, Kwon D, Ma B, et al. Appl Phys Lett 2008;92 252905-1–3.
[8] Schwartz RW. Chem Mater 1997;9:2325–40.
[9] Nagarajan V, Roytburd A, Stanishevsky A, et al. Nat Mater 2002;2:43–7.
[10] Janolin PE. J Mater Sci 2009;44:5025–48.
[11] Hwang CS, Lee BT, Kang CS, et al. J Appl Phys 1999;85:287–95.
[12] Streiffer SK, Basceri C, Parker CB, et al. J Appl Phys 1999;86:4565–7.
[13] Nagarajan V, Alpay SP, Ganpule CS, et al. Appl Phys Lett 2000;77:438–40.
[14] Taylor TR, Hansen PJ, Acikel B, et al. Appl Phys Lett 2002;80:1978.
[15] Shaw TM, Suo Z, Huang M, et al. Appl Phys Lett 1999;75:2129–31.
[16] Catalan G, Corbett M, Bowman R, et al. J Appl Phys 2002;91:2295.
[17] Tong S, Ma B, Narayanan M, et al. ACS Appl Mater Interfaces 2013;5:1474–80.
[18] Dube DC, Baborowski J, Muralt P, et al. Appl Phys Lett 1999;74:3546.
[19] Tyunina M. J Phys: Condens Matter 2006;18:5725–38.
[20] Narayanan M, Balachandran U, Stoupin S, et al. J Phys D 2012;45:335401.
[21] Lu S, Zuo C, Zeng H, et al. Mater Lett 2006;60:255–60.
[22] Dawber M, Rabe KM, Scott JF. Rev Mod Phys 2005;77:1083–130.
[23] Tong S, Narayanan M, Ma B, et al. Acta Mater 2011;59:1309–16.
[24] Ma B, Tong S, Narayanan M, et al. Mater Res Bull 2011.
[25] Welzel U, Ligot J, Lamparter P, et al. J Appl Crystallogr 2005;38:1–29.
[26] Narayanan M, Ma B, Balachandran U, et al. J Appl Phys 2010;107:024103.
[27] Haertling GH. J Am Ceram Soc 1971;54:303–9.
[28] Weast RC, Astle MJ, Beyer WH. CRC Handbook of Chemistry and Physics. FL: CRC Press Boca Raton; 1988.
[29] Balachandran U, Kwon DK, Narayanan M, et al. J Eur Ceram Soc 2010;30:365–8.